JOURNAL OF THERMOPHYSICS AND HEAT TRANSFER
Vol. 20, No. 1, January–March 2006

# Technical Notes

*TECHNICAL NOTES are short manuscripts describing new developments or important results of a preliminary nature. These Notes should not exceed 2500 words (where a figure or table counts as 200 words). Following informal review by the Editors, they may be published within a few months of the date of receipt. Style requirements are the same as for regular contributions (see inside back cover).*

## Meshless Local Petrov–Galerkin Method for Solving Radiative Transfer Equation

L. H. Liu*
*Harbin Institute of Technology,*
*150001 Harbin, People's Republic of China*

### Nomenclature

| | | |
|---|---|---|
| $\bar{\boldsymbol{A}}$ | = | matrix defined in Eq. (7) |
| $a$ | = | Coefficients for the moving least-squares (MLS) approximation in Eq. (4) |
| $\boldsymbol{a}$ | = | vector of coefficient $a$ |
| $\boldsymbol{B}$ | = | matrix defined in Eq. (8) |
| $C_j$ | = | expansion coefficient of scattering phase function |
| $f$ | = | coefficients in linear equations |
| $g$ | = | quartic spline function defined in Eq. (17) |
| $I$ | = | radiative intensity, W/m$^3$ · sr |
| $I_b$ | = | blackbody radiative intensity, W/m$^3$ · sr |
| $\tilde{I}$ | = | MLS approximant of radiative intensity, W/m$^3$ · sr |
| $\hat{I}$ | = | fictitious radiative intensity, W/m$^3$ · sr |
| $\hat{\boldsymbol{I}}$ | = | vector of trial function defined in Eq. (9) |
| $J$ | = | weighted discrete $L_2$ norm defined in Eq. (5) |
| $K$ | = | coefficients in linear equations |
| $k$ | = | order of monomial basis |
| $L$ | = | slab thickness, side length of rectangular medium, m |
| $l$ | = | spatial coordinate |
| $M$ | = | number of discrete ordinates |
| $N$ | = | number of nodes in the problem domain |
| $n$ | = | node number in subdomain $V_x$ |
| $\boldsymbol{n}$ | = | unit normal vector |
| $P_j$ | = | legendre polynomial of order $j$ |
| $\boldsymbol{p}$ | = | complete monomial basis |
| $p_j$ | = | monomial basis function of order $j$ |
| $q$ | = | radiative heat flux, W/m$^2$ |
| $r$ | = | dimensionless distance |
| $\boldsymbol{s}$ | = | unit vector of discrete ordinate |
| $T$ | = | temperature, K |
| $T_g$ | = | medium temperature, K |
| $T_1, T_2$ | = | temperature at the plate ends, K |
| $V$ | = | volume of subdomain |
| $V_S$ | = | local subdomain for weighted integration |
| $V_x$ | = | definition domian of MLS approximation for the trial function at $\boldsymbol{x}$ |
| $v$ | = | test function |
| $w$ | = | weight corresponding to discrete ordinate |
| $w^{\mathrm{MLS}}$ | = | MLS weight function |
| $x, y, z$ | = | cartesian coordinates |
| $\boldsymbol{x}$ | = | spatial position vector of point, $[x, y, z]^T$ |
| $\boldsymbol{x}_Q$ | = | gaussian quadrature point |
| $\alpha_{GQ}$ | = | dimensionless size parameter for the Gaussian quadrature |
| $\alpha_{\mathrm{MLS}}$ | = | dimensionless size parameter for the MLS approximation |
| $\Delta x, \Delta y$ | = | average nodal spacing between two neighboring nodes in the $x$ and $y$ coordinate directions |
| $\varepsilon$ | = | emissivity |
| $\Theta$ | = | nondimensional temperature |
| $\kappa$ | = | absorption coefficient, m$^{-1}$ |
| $\mu, \eta, \xi$ | = | direction cosine of discrete ordinate |
| $\sigma$ | = | scattering coefficient, m$^{-1}$ |
| $\bar{\sigma}$ | = | stefan–Boltzmann constant, W/m$^2$ · K$^4$ |
| $\tau_L$ | = | optical thickness, $(\kappa + \sigma)L$ |
| $\Phi$ | = | scattering phase function |
| $\phi$ | = | shape function of MLS approximation |
| $\omega$ | = | single scattering albedo, $\omega = \kappa/(\kappa + \sigma)$ |

*Subscripts*

| | | |
|---|---|---|
| $i$ | = | value at node $i$ |
| $Q$ | = | gaussian quadrature point |
| $w$ | = | value on boundary |

*Superscript*

| | | |
|---|---|---|
| $m, m'$ | = | discrete ordinate direction |

### Introduction

NUMERICAL solutions of the radiative transfer equation, in an absorbing, emitting, and scattering medium require considerable effort for most practical systems composed of semitransparent media. Recently, many numerical methods have been developed to solve the problem of radiative heat transfer in semitransparent media. Examples are the Monte Carlo method, the zonal method, the discrete-ordinates method (DOM), the finite volume method (FVM), and the finite element method (FEM).[1,2] Because the domain of the problem needs to be discretized, these traditional methods, especially the FEM, suffer from drawbacks such as tedious meshing and remeshing.

In the computational mechanics community, many meshless methods have been proposed for computational mechanics problems to avoid the tedious meshing and remeshing. The meshless method is used to establish a system of algebraic equations for the whole problem domain without the use of a predefined mesh. Meshless methods use a set of nodes scattered within the problem domain and its boundaries. These scattered nodes do not form a mesh, which means that no information on the relationship among the nodes is required. Various methods belonging to this family are the element-free Galerkin method, the meshless local Petrov–Galerkin (MLPG) method, the point interpolation method, smoothed particle hydrodynamics method, and so on (see Refs. 3–5). Among these methods, the MLPG method is a truly meshless method, which was originated by Atluri and Zhu.[6] To the best of the author's knowledge, meshless methods have not been used for radiative heat transfer.

Received 29 November 2004; revision received 3 May 2005; accepted for publication 8 May 2005. 

*Professor, School of Energy Science and Engineering, 92 West Dazhi Street; lhliu@hit.edu.cn.

In this Note, we develop an MLPG method for radiative heat transfer based on the discrete-ordinates equation. Three cases of radiative heat transfer in semitransparent media are examined to verify the accuracy of this new solution method.

## Mathematical Formulation

Consider radiative transfer in a semitransparent enclosure. The discrete-ordinates equation of radiative transfer can be written as[1,2]

$$\mu^m \frac{\partial I^m}{\partial x} + \eta^m \frac{\partial I^m}{\partial y} + \xi^m \frac{\partial I^m}{\partial z} = -(\kappa + \sigma) I^m + \kappa I_b + \frac{\sigma}{4\pi} \sum_{m'=1}^{M} I^{m'} \Phi^{m'm} w^{m'} \tag{1}$$

with boundary conditions

$$I_w^m = \varepsilon_w I_{bw} + \frac{1 - \varepsilon_w}{\pi} \sum_{n_w \cdot s^{m'} < 0} I_w^{m'} \left| \boldsymbol{n}_w \cdot \boldsymbol{s}^{m'} \right| w^{m'} \tag{2}$$

When the forward scattering term is moved from the right side of Eq. (1) to the left side, Eq. (1) can be rewritten as [7]

$$\mu^m \frac{\partial I^m}{\partial x} + \eta^m \frac{\partial I^m}{\partial y} + \xi^m \frac{\partial I^m}{\partial z} + \left( \kappa + \sigma - \frac{\sigma}{4\pi} \Phi^{mm} w^m \right) I^m = \kappa I_b + \frac{\sigma}{4\pi} \sum_{m'=1, m' \neq m}^{M} I^{m'} \Phi^{m'm} w^{m'} \qquad m = 1, 2, \ldots, M \tag{3}$$

### MLS Approximation

In the MLPG implementation, a moving least-squares (MLS) approximation[3–6] is employed for constructing shape functions to approximate the radiative intensity. Consider a spatial subdomain $V_x$ in the neighborhood of a point $\boldsymbol{x}$ and denoted as the domain of definition of the MLS approximation for the trial function at $\boldsymbol{x}$, which is located within the problem domain. To approximate the distribution of radiative intensity $I^m$ in $V_x$, over a number of local nodes $\{\boldsymbol{x}_i\}$, $i = 1, 2, \ldots, n$, the MLS approximant $\tilde{I}^m(\boldsymbol{x})$ of $I^m$, $\forall \boldsymbol{x} \in V_x$, can be defined by

$$\tilde{I}^m = \sum_{j=0}^{k} p_j(\boldsymbol{x}) a_j(\boldsymbol{x}) = \boldsymbol{p}^T(\boldsymbol{x}) \boldsymbol{a}(\boldsymbol{x}) \tag{4}$$

where $\boldsymbol{p}^T(\boldsymbol{x}) = [p_1(\boldsymbol{x}), p_2(\boldsymbol{x}), \ldots, p_k(\boldsymbol{x})]$ is a complete monomial basis of order $k$ and $\boldsymbol{a}(\boldsymbol{x})$ is a vector containing coefficients $a_j(\boldsymbol{x})$, $j = 1, 2, \ldots, k$, which are functions of the spatial coordinates $\boldsymbol{x} = [x, y, z]^T$. The coefficient vector $\boldsymbol{a}(\boldsymbol{x})$ is determined by minimizing a weighted discrete $L_2$ norm, defined as

$$J[\boldsymbol{a}(\boldsymbol{x})] = \sum_{i=1}^{n} w_i^{\mathrm{MLS}} \left[ \boldsymbol{p}^T(\boldsymbol{x}_i) \boldsymbol{a}(\boldsymbol{x}) - \hat{I}_i^m \right]^2 \tag{5}$$

where $\boldsymbol{x}_i$ is the value of $\boldsymbol{x}$ at node $i$; $w_i^{\mathrm{MLS}}(\boldsymbol{x})$ is the MLS weight function associated with node $i$, with $w_i^{\mathrm{MLS}}(\boldsymbol{x}) > 0$ for all $\boldsymbol{x}$ in the support domain $V_x$ of $w_i^{\mathrm{MLS}}(\boldsymbol{x})$; and $n$ is the number of nodes in $V_x$ for which the weight functions $w_i^{\mathrm{MLS}}(\boldsymbol{x}) > 0$. Here, $\hat{I}_i^m$ in Eq. (5) is a fictitious nodal value and not the nodal value, of the unknown trial function $\tilde{I}_i^m$ in general.

Minimizing of $J$ with respect to $\boldsymbol{a}(\boldsymbol{x})$ leads to the following linear relation between $\boldsymbol{a}(\boldsymbol{x})$ and $\hat{\boldsymbol{I}}^m$:

$$\boldsymbol{A}(\boldsymbol{x}) \boldsymbol{a}(\boldsymbol{x}) = \boldsymbol{B}(\boldsymbol{x}) \hat{\boldsymbol{I}}^m \tag{6}$$

where the matrices $\boldsymbol{A}(\boldsymbol{x})$, $\boldsymbol{B}(\boldsymbol{x})$, and $\hat{\boldsymbol{I}}^m$ are defined by

$$\boldsymbol{A}(\boldsymbol{x}) = \sum_{i=1}^{n} w_i^{\mathrm{MLS}}(\boldsymbol{x}) \boldsymbol{p}(\boldsymbol{x}_i) \boldsymbol{p}^T(\boldsymbol{x}_i) \tag{7}$$

$$\boldsymbol{B}(\boldsymbol{x}) = \left[ w_1^{\mathrm{MLS}}(\boldsymbol{x}) \boldsymbol{p}(\boldsymbol{x}_1), w_2^{\mathrm{MLS}}(\boldsymbol{x}) \boldsymbol{p}(\boldsymbol{x}_2), \ldots, w_n^{\mathrm{MLS}}(\boldsymbol{x}) \boldsymbol{p}(\boldsymbol{x}_n) \right] \tag{8}$$

$$\hat{\boldsymbol{I}}^m = \left[ \hat{I}_1^m, \hat{I}_2^m, \ldots, \hat{I}_n^m \right] \tag{9}$$

Solving for $\boldsymbol{a}(\boldsymbol{x})$ from Eq. (6) and substituting into Eq. (4) gives a relation that may be written in the form of an interpolation function similar to that used in FEM, as

$$\tilde{I}^m(\boldsymbol{x}) = \sum_{i=1}^{n} \phi_i(\boldsymbol{x}) \hat{I}_i^m, \qquad \forall \boldsymbol{x} \in V_x \tag{10}$$

where

$$\phi_i(\boldsymbol{x}) = \sum_{j=1}^{k} p_j(\boldsymbol{x}) [\boldsymbol{A}^{-1}(\boldsymbol{x}) \boldsymbol{B}(\boldsymbol{x})]_{ji} \tag{11}$$

where $\phi_i(\boldsymbol{x})$ is usually termed the shape function of the MLS approximation corresponding to nodal point $\boldsymbol{x}_i$. The partial derivative of the shape function is obtained as

$$\phi_{i,l}(\boldsymbol{x}) = \sum_{j=1}^{k} \left\{ p_{j,l} [\boldsymbol{A}^{-1} \boldsymbol{B}]_{ji} + p_j \left[ \boldsymbol{A}^{-1} \boldsymbol{B}_{,l} + (\boldsymbol{A}^{-1})_{,l} \boldsymbol{B} \right]_{ji} \right\} \tag{12}$$

where $(\,)_{,l} = \partial(\,)/\partial l$ represents the derivative with respect to spatial coordinate $l$ and $l = x, y, z$.

### Discretization and Numerical Implementation

Equation (3) is weighted over the local subdomain $V_S$, which is located entirely inside the global problem domain. The local subdomain $V_S$ can be taken to be a sphere or cube (for three-dimensional problems) centered at the point $\boldsymbol{x}_i$ in question. The integrated residuals are set to zero,

$$\int_{V_S} \left[ \mu^m \frac{\partial I^m}{\partial x} + \eta^m \frac{\partial I^m}{\partial y} + \xi^m \frac{\partial I^m}{\partial z} + \left( \kappa + \sigma - \frac{\sigma}{4\pi} \Phi^{mm} w^m \right) I^m - \left( \kappa I_b + \frac{\sigma}{4\pi} \sum_{m'=1, m' \neq m}^{M} I^{m'} \Phi^{m'm} w^{m'} \right) \right] v(\boldsymbol{x} - \boldsymbol{x}_i)\, \mathrm{d}V = 0 \qquad i = 1, 2, \ldots, N \tag{13}$$

Substitution of Eqs. (10–12) into Eq. (13) for all nodes leads to the following discretized system of linear equations:

$$\sum_{j=1}^{N} K_{ij}^m I_j^m = f_i^m, \qquad i = 1, 2, \ldots, N \tag{14}$$

where

$$K_{ij}^m = \int_{V_S} \left[ \mu^m \phi_{j,x}(\boldsymbol{x}) + \eta^m \phi_{j,y}(\boldsymbol{x}) + \xi^m \phi_{j,z}(\boldsymbol{x}) + \left( \kappa + \sigma - \frac{\sigma}{4\pi} \Phi^{mm} w^m \right) \phi_j(\boldsymbol{x}) \right] v(\boldsymbol{x} - \boldsymbol{x}_i)\, \mathrm{d}V \tag{15a}$$

$$f_i^m = \int_{V_S} \left( \kappa I_b + \frac{\sigma}{4\pi} \sum_{m'=1, m' \neq m}^{M} I^{m'} \Phi^{m'm} w^{m'} \right) v(\boldsymbol{x} - \boldsymbol{x}_i)\, \mathrm{d}V \tag{15b}$$

Equation (14) is solved independently for each direction, and the boundary conditions (2) must be imposed on the inflow boundary. For each node $i$ on the inflow boundary, the radiative intensity $I_i^m$ is given by boundary conditions (2), and the boundary condition can be directly imposed as follows:

$$K_{ij}^m = \begin{cases} 1, & i = j \\ 0, & i \neq j \end{cases} \tag{16a}$$

$$f_i^m = I_i^m \tag{16b}$$

Because the in-scattering term of the discrete-ordinates equation in direction $m$ contains the radiative intensities of the other directions, global iterations similar to those used in DOM are necessary to include the source and boundary conditions.

The implementation of the MLPG method can be carried out according to the following routine.

1) Choose a finite number of nodes in the problem domain and its boundaries; choose the basis function MLS weight function, and test function such that the MLS approximation is well defined and weighted integration of the radiative transfer equation can be implemented.

2) Determine the local subdomain $V_S$ and its boundary for each node and calculate the Gaussian quadrature points $\boldsymbol{x}_Q$ in $V_S$.

3) Determine the nodes $\boldsymbol{x}_i$ located in the domain of definition of the MLS approximation for the trial function at point $\boldsymbol{x}_Q$, that is, those nodes with $w_i^{\mathrm{MLS}}(\boldsymbol{x}_Q) > 0$.

4) For those nodes in the domain of definition of the MLS approximation of the trial function at point $\boldsymbol{x}_Q$, calculate shape function $\phi_i(\boldsymbol{x}_Q)$ and the derivatives $\phi_{i,x}(\boldsymbol{x}_Q)$, $\phi_{i,y}(\boldsymbol{x}_Q)$, and $\phi_{i,z}(\boldsymbol{x}_Q)$.

5) Calculate the boundary condition given by Eq. (2). Evaluate the numerical integrals in Eqs. (15a) and (15b), and assemble contributions to the linear system of Eq. (14) for all nodes.

6) Solve the linear system of Eq. (14) for the fictitious nodal values $\hat{I}^m$.

7) Terminate the iteration process if the specified stopping criterion is satisfied. Otherwise, go back to step 5.

In this Note, the maximum relative error, $10^{-4}$, of the radiative intensity is taken as the stopping criterion for iteration.

## Results and Discussion

To verify the accuracy of the MLPG approach already presented, three test cases for radiative heat transfer are examined. The test cases are selected because exact, or at least very precise, solutions of the radiative transfer equation exist for comparison with the MLPG approach. For the following numerical study, the equal weight even quadrature $S_6$ is selected, and a quartic spline function is used to construct the weight function for the MLS approximation and the test function in the weighted integration of radiative transfer equation. The quartic spline function is given as follows:

$$g(r) = \begin{cases} 1 - 6r^2 + 8r^3 - 3r^4, & r \le 1 \\ 0, & r > 1 \end{cases} \tag{17}$$

where $r$ is the dimensionless distance.

### Case 1: Nonscattering Gray Medium Between Parallel Black Plates

The MLPG approach is applied to solve for the temperature distribution in a nonscattering gray medium between parallel black plates. The temperatures of the plates are $T_1$ and $T_2$, respectively. There are 51 nodes uniformly distributed in the problem domain and its boundaries. The monomial basis $\boldsymbol{p}^T(\boldsymbol{x}) = [1, x, x^2]$ is used, and the weight function for the MLS approximation and the test function in the weighted integration of the radiative transfer equation are given as follows:

$$w^{\mathrm{MLS}}(x - x_i) = g\left(\left|\frac{x - x_i}{\alpha_{\mathrm{MLS}}\Delta x}\right|\right) \tag{18a}$$

$$v(x - x_i) = g\left(\left|\frac{x - x_i}{\alpha_{GQ}\Delta x}\right|\right) \tag{18b}$$

where $\Delta x$ is the average nodal spacing between two neighboring nodes and the dimensionless size parameters $\alpha_{\mathrm{MLS}} = 2.5$ and $\alpha_{GQ} = 1.5$ are used.

The nondimensional temperature distribution $\Theta = (T^4 - T_2^4)/(T_1^4 - T_2^4)$ in the gray medium at radiative equilibrium is presented in Fig. 1 for three different optical thicknesses $\tau_L$, namely, 0.1, 1, and 10, and compared with the exact solution obtained by Heaslet and Warming.[8] The MLPG results agree with the exact values very well. The maximum relative error based on the data in Ref. 8 is less than 4%. The time required for computation is less than 1 min on a personal computer with an Athlon XP2000 + 1.67-GHz processor.

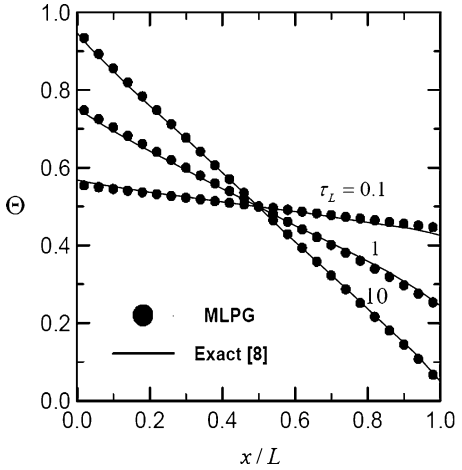


**Fig. 1 Nondimensional temperature distribution in gray medium at radiative equilibrium between parallel black plates.**

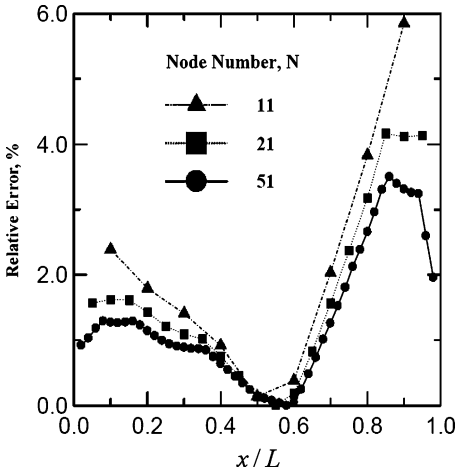


**Fig. 2 Effects of node number on solution accuracy.**

The effect of node number is shown in Fig. 2 for the case of $\tau_L = 1$. The relative error based on the exact data in Ref. 8 is defined as

$$\text{relative error} = 100 \times \left|\frac{\text{data obtained by MPLG} - \text{exact value in Ref. 8}}{\text{exact value in Ref. 8}}\right| \tag{19}$$

As shown in Fig. 2, the comparison is quite good, even with a node number of only $N = 11$. The convergence of the MLPG is demonstrated in Fig. 2.

### Case 2: Anisotropically Scattering in a Black Enclosure

We consider radiative heat transfer in a two-dimensional rectangular gray semitransparent medium enclosed by black boundaries. The optical thickness based on the side length $L$ of the rectangular enclosure is $\tau_L = 1.0$. The medium is kept hot, but the temperatures of all boundary walls are maintained at 0 K. The temperature $T_g$, the absorption coefficient $\kappa$, and the scattering coefficient $\sigma$ of the medium enclosed by the rectangular enclosure are uniform. Kim and Lee [9] studied the case using DOM, and Liu [10] studied the case using FEM. The following phase function[7] with asymmetry factor 0.66972 is used:

$$\Phi = \sum_{j=0}^{8} C_j P_j(\mu) \tag{20}$$

where the $P_j$ are Legendre polynomials. The $C_j$ are the expansion coefficients defined as $C_0 = 1.0$, $C_1 = 2.00917$, $C_2 = 1.56339$,

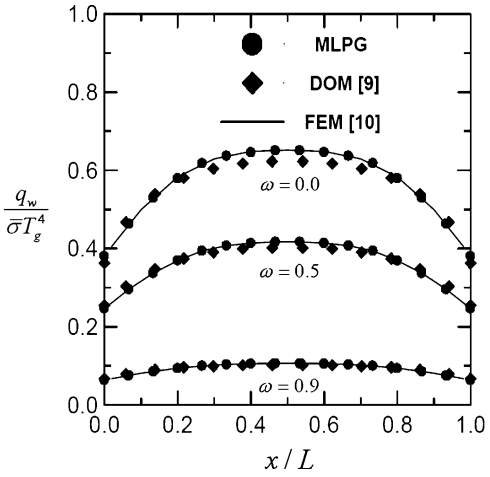


**Fig. 3 Nondimensional net radiative heat flux on the lower wall in rectangular enclosure.**

$C_3 = 0.67407$, $C_4 = 0.22215$, $C_5 = 0.04725$, $C_6 = 0.00671$, $C_7 = 0.00068$ and $C_8 = 0.00005$.

The MLPG approach is applied to this case, and 256 nodes are uniformly distributed within the problem domain and on its boundaries. The monomial basis $\boldsymbol{p}^T(\boldsymbol{x}) = [1, x, y, x^2, xy, y^2]$ is used, and the weight function for the MLS approximation and the test function in the weighted integration of radiative transfer equation are given as follows:

$$w^{\mathrm{MLS}}(\boldsymbol{x} - \boldsymbol{x}_i) = g\left(\left|\frac{x - x_i}{\alpha_{\mathrm{MLS}}\Delta x}\right|\right) g\left(\left|\frac{y - y_i}{\alpha_{\mathrm{MLS}}\Delta y}\right|\right) \tag{21a}$$

$$v(\boldsymbol{x} - \boldsymbol{x}_i) = g\left(\left|\frac{x - x_i}{\alpha_{GQ}\Delta x}\right|\right) g\left(\left|\frac{y - y_i}{\alpha_{GQ}\Delta y}\right|\right) \tag{21b}$$

where $\Delta x$ and $\Delta y$ are the average nodal spacings between two neighboring nodes in the $x$ and $y$ coordinate directions, respectively, and the dimensionless size parameters $\alpha_{\mathrm{MLS}} = 2.5$ and $\alpha_{GQ} = 1.5$ are used.

The nondimensional net radiative heat fluxes $q_w/\bar{\sigma}T_g^4$ on the lower wall are shown in Fig. 3 for three values of single scattering albedo $\omega$, namely, 0.0, 0.5, and 0.9, and compared to the results obtained from DOM [9] and FEM.[10] By comparison, it can be seen that the MLPG approach presented in this Note has good accuracy in solving for the radiative heat transfer in anisotropically scattering media. The MLPG results are very close to those obtained from the FEM. Similar to the FEM, the MLPG results differ from those of the DOM to some extent. Even in the case of $\omega = 0.0$, the maximum relative error based on the DOM data in Ref. 9 is less than 7%, and the maximum relative error based on the FEM data in Ref. 10 is less than 2%.

#### Case 3: Nonscattering Gray Medium in a Trapezoidal Enclosure

As shown in Fig. 4, we consider the radiative heat transfer in a two-dimensional trapezoidal gray semitransparent medium enclosed by black boundaries. The width of the bottom wall is $L = 1$ m. The medium is kept hot, but the temperatures of all boundary walls are maintained at 0 K. The temperature $T_g$ and the absorption coefficient of the medium enclosed by the rectangular enclosure are uniform. Byun et al. [11] studied the case using embedded FVM.

As shown in Fig. 4, 169 MPLG nodes are uniformly distributed within the problem domain and on its boundaries. The monomial basis, the weight function, for the MLS approximation, the test function, and the dimensionless size parameters are same as those used in case 2. The nondimensional net radiative heat fluxes $q_w/\bar{\sigma}T_g^4$ on the lower wall are shown in Fig. 5 for two different values of absorption coefficient, namely, $\kappa = 1.0\ \mathrm{m}^{-1}$ and $\kappa = 0.1\ \mathrm{m}^{-1}$, and are compared to the exact solution[11] and to the results obtained from the embedded FVM. By comparison, it can be seen that the MLPG

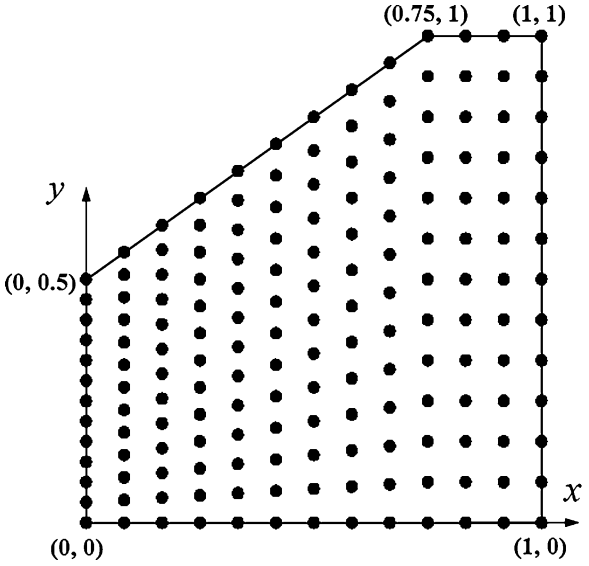


**Fig. 4 Schematic and node system of trapezoidal enclosure.**

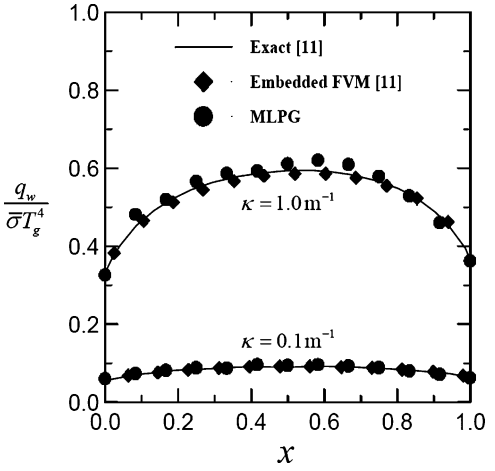


**Fig. 5 Nondimensional net radiative heat flux on lower wall in trapezoidal enclosure.**

approach presented in this Note has good accuracy in solving for the radiative heat transfer in complex geometries. The maximum relative error based on the exact data in Ref. 11 is less than 7%. The time required for computation is less than 15 min on a personal computer with an Athlon XP2000 + 1.67-GHz processor.

## Conclusions

An MLPG method based on the discrete-ordinates equation is developed for the simulation of radiative heat transfer in absorbing and scattering media. Three cases of radiative heat transfer in semitransparent media are examined to verify the accuracy of this new method. The results show that the MLPG approach presented in this Note has good accuracy in solving for the radiative heat transfer in absorbing and scattering media. In comparison with traditional numerical methods for radiative heat transfer, such as the Monte Carlo method, the zonal method, the DOM, the FVM, and the FEM, the MLPG approach avoids complex and time-consuming meshing and remeshing processes and can be used to solve for the radiative heat transfer in anisotropically scattering media.

## Acknowledgment

The support of this work by the National Nature Science Foundation of China (50336010) is gratefully acknowledged.

## References

[1]Modest, M. F., *Radiative Heat Transfer*, 2nd ed., Academic Press, San Diego, CA, 2003, pp. 498–564.

[2]Siegel, R., and Howell, J. R., *Thermal Radiation Heat Transfer*, 4th ed., Taylor and Francis, New York, 2002, pp. 663–776.

[3]Liu, G. R., *Mesh Free Methods*, CRC Press, Boca Raton, FL, 2003, pp. 67–248.

[4]Zhang, X., and Liu, Y., *Meshless Methods*, Tsinghua Univ. Press, Beijing, 2004, pp. 144–176.

[5]Atluri, S. N., and Shen, S. P., *The Meshless Local Petrov–Galerkin (MLPG) Method*, Tech Science, Encino, CA, 2002, pp. 93–214.

[6]Atluri, S. N., and Zhu, T., "A New Meshless Local Petrov–Galerkin (MLPG) Approach in Computational Mechanics," *Computational Mechanics*, Vol. 22, No. 2, 1998, pp. 117–127.

[7]Chai, J. C., Lee, H. S., and Patankar, S. V., "Improved Treatment of Scattering Using the Discrete Ordinates Method," *Journal of Heat Transfer*, Vol. 116, No. 1, 1994, pp. 260–263.

[8]Heaslet, M. A., and Warming, R. F., "Radiative Transport and Wall Temperature Slip in an Absorbing Planar Medium," *International Journal of Heat and Mass Transfer*, Vol. 8, No. 7, 1965, pp. 979–994.

[9]Kim, T. K., and Lee, H., "Effect of Anisotropic Scattering on Radiative Heat Transfer in Two-Dimensional Rectangular Enclosures," *International Journal of Heat and Mass Transfer*, Vol. 31, No. 8, 1988, pp. 1711–1721.

[10]Liu, L. H., "Finite Element Simulation of Radiative Heat Transfer in Absorbing and Scattering Media," *Journal of Thermophysics and Heat Transfer*, Vol. 18, No. 4, 2004, pp. 555–557.

[11]Byun, D. Y., Baek, S. W., and Kim, M. Y., "Prediction of Radiative Heat Transfer in a 2D enclosure with Blocked-off, Multi-block, and Embeded Boundary Treatments," *Proceedings of ASME Heat Transfer Division*, HTD-Vol. 366-1, American Society of Mechanical Engineers, Fairfield, NJ, 2000, pp. 119–126.